

The role of stellar mass and environment for cluster blue fraction, AGN fraction and star formation indicators from a targeted analysis of Abell 1691

Kevin A. Pimbblet^{1,2★} and Peter C. Jensen³

¹*School of Physics, Monash University, Clayton, Victoria 3800, Australia*

²*Monash Centre for Astrophysics (MoCA), Monash University, Clayton, Victoria 3800, Australia*

³*Centre for Astrophysics and Supercomputing, Swinburne University of Technology, Hawthorn, Victoria 3122, Australia*

Accepted 2012 August 2. Received 2012 August 1; in original form 2012 February 6

ABSTRACT

We present an analysis of the galaxy population of the intermediate X-ray luminosity galaxy cluster, Abell 1691, from Sloan Digital Sky Survey (SDSS) and Galaxy Zoo data to elucidate the relationships between environment and galaxy stellar mass for a variety of observationally important cluster populations that include the Butcher–Oemler blue fraction, the active galactic nucleus (AGN) fraction and other spectroscopic classifications of galaxies. From 342 cluster members, we determine a cluster recession velocity of $21257 \pm 54 \text{ km s}^{-1}$ and velocity dispersion of $1009^{+40}_{-36} \text{ km s}^{-1}$ and show that although the cluster is fed by multiple filaments of galaxies it does not possess significant sub-structure in its core. We identify the AGN population of the cluster from a Baldwin, Phillips & Terlevich diagram and show that there is a mild increase in the AGN fraction with radius from the cluster centre that appears mainly driven by high-mass galaxies [$\log(\text{stellar mass}) > 10.8$]. Although the cluster blue fraction follows the same radial trend, it is caused primarily by lower mass galaxies [$\log(\text{stellar mass}) < 10.8$]. Significantly, the galaxies that have undergone recent starbursts or are presently starbursting but dust-shrouded [spectroscopic e(a) class galaxies] are also nearly exclusively driven by low-mass galaxies. We therefore suggest that the Butcher–Oemler effect may be a mass-dependent effect. We also examine red and passive spiral galaxies and show that the majority are massive galaxies, much like the rest of the red and spectroscopically passive cluster population. We further demonstrate that the velocity dispersion profiles of low- and high-mass cluster galaxies are different. Taken together, we infer that the duty cycle of high- and low-mass cluster galaxies is markedly different, with a significant departure in star formation and specific star formation rates observed beyond r_{200} and we discuss these findings.

Key words: galaxies: active – galaxies: clusters: individual: Abell 1691 – galaxies: evolution – galaxies: stellar content.

1 INTRODUCTION

Arguably the most important, emergent conclusion about galaxy evolution during the past decade is that the two main driving forces behind it are the stellar mass of a galaxy and its large-scale environment. Although stellar mass may be the more important of the pair, the environmental effects are also non-negligible and the two variables likely exhibit a significant covariance (Baldry et al. 2006; see also von der Linden et al. 2010).

For example, in the extreme (and hostile) environment of the dense cores of massive galaxy clusters galaxy colour is preferen-

tially red and galaxy morphology elliptical – a systematic difference to non-cluster galaxies (e.g. Dressler 1980; Dressler et al. 1997; Lewis et al. 2002; Gómez et al. 2003; Balogh et al. 2004a,b; Kauffmann et al. 2004; Christlein & Zabludoff 2005; Baldry et al. 2006; Cooper et al. 2006; Pimbblet et al. 2006; Sato & Martin 2006; Bamford et al. 2009; Skibba et al. 2009; Deng et al. 2010; Peng et al. 2010; Ma & Ebeling 2011; Patel et al. 2011; Calvi et al. 2012; Jensen & Pimbblet 2012).

The mass function of cluster galaxies shows that the more massive galaxies are also redder and more frequently elliptical (e.g. Baldry et al. 2006; di Serego Alighieri, Lanzoni & Jørgensen 2006; Clemens et al. 2006; van der Wel et al. 2007; van den Bosch et al. 2008; Bamford et al. 2009; Deng et al. 2010; Pasquali et al. 2010; Peng et al. 2010; Nair & Abraham 2010; Thomas et al. 2010;

★E-mail: kevin.pimbblet@monash.edu

Grützbauch et al. 2011; Giodini et al. 2012; Wilman & Erwin 2012; see also Vulcani et al. 2012).

Early investigations into galaxy evolution inside clusters of galaxies by Butcher & Oemler (1978, 1984) suggested that the fraction of blue galaxies decreases rapidly with decreasing redshift. They hypothesized that the cause of this dramatic change in blue fraction to be due to spiral galaxies undergoing ram-pressure stripping caused by interaction with the intra-cluster environment (e.g. Gunn & Gott 1972). Such spirals morphologically transform into lenticular (S0) galaxies and fade as they are no longer able to replenish their gas supplies. Later works confirmed the existence of the Butcher–Oemler effect (Couch et al. 1994; Rakos & Schombert 1995; Lubin 1996; Dressler et al. 1997; Smail et al. 1998; Ellingson et al. 2001; Kodama & Bower 2001; Margoniner et al. 2001; Goto et al. 2003a; Tran et al. 2003; De Propriis et al. 2004; Urquhart et al. 2010). Yet, observational follow-up by Dressler & Gunn (1983) demonstrated that the blue galaxies measured by the Butcher–Oemler effect are actually undergoing starbursts rather than gently fading away, indicating that instead of gas being stripped in a galaxy, it could be used up in a spectacular, albeit terminal, starburst phase. Couch & Sharples (1987) made an independent spectroscopic study of $z \approx 0.3$ clusters and came to the same conclusion: the blue galaxies are being driven by galaxies that have undergone a recent (explicitly: within 0.5 Gyr) starburst. This observational conclusion has been re-enforced by later studies (e.g. Lavery & Henry 1988; Couch et al. 1994, 1998; Fabricant, Bautz & McClintock 1994; Abraham et al. 1996; Fisher et al. 1998; Poggianti et al. 1999; Dressler et al. 2004). Moreover, some of the other cluster galaxies also exhibited the rare signatures of a post-starburst phase (E+A galaxies; e.g. Zabludoff et al. 1996), suggesting a duty cycle for these blue galaxies (see also Mahajan, Haines & Raychaudhury 2010). The cause of the blue Butcher–Oemler galaxies has subsequently been argued to be due to a number of different physical mechanisms including, but not limited to, galaxy–galaxy interaction (Lavery & Henry 1988; Couch et al. 1994; Moore et al. 1996; Quilis, Moore & Bower 2000), galaxy–cluster interaction (Henriksen & Byrd 1996; Bekki, Couch & Shioya 2001), galaxy mergers (Dressler et al. 1999; van Dokkum et al. 1999) or a slow starvation of star-forming gas (Larson, Tinsley & Caldwell 1980; Balogh & Morris 2000; Bekki, Couch & Shioya 2002). These mechanisms operate most efficiently in different environments which would lead to differentiable observational signatures (e.g. ram pressure induced starbursts should cause more blue galaxies close to the cluster core, whereas mergers would not do so).

We caution here, however, that there are certainly observational biases affecting some studies (as indicated by Andreon & Etori 1999; De Propriis et al. 2003; Andreon et al. 2006; Holden et al. 2007), claims of a lack of Butcher–Oemler effect (e.g. Andreon et al. 2006; Haines et al. 2009) or at the very least a dampened effect when some of these selection biases are taken into account (cf. Margoniner & de Carvalho 2000). For example, if galaxies are mass selected, then bluer galaxies are seldom found in more massive regimes ($>10^{11}$ solar masses; see Raichoor & Andreon 2012a,b).

Taking the above results together, it is suggestive that a starbursting phase is very important in the evolution (or duty cycle) of cluster galaxies (Oemler et al. 2009) – especially at lower masses (Mahajan et al. 2010). As galaxies accrete on to the cluster potential, *some* may experience a starburst due to one or more of the above mechanisms (see also Fadda et al. 2008; Porter et al. 2008). Whilst galaxies outside a cluster tend to revert to their long-term star formation rates after a starburst, cluster galaxies do not (cf. Poggianti et al. 1999; Dressler et al. 2004; Oemler et al. 2009; see also Dressler et al.

2009). The duty cycle of cluster galaxies therefore merits further investigation at all redshifts – particularly if we are to elucidate the connections between mass, environment, colour and morphology that we have summarized above. We can also tie these relationships to incidence of active galactic nuclei (AGN). From a simplistic observational viewpoint, powerful AGN are found in massive galaxies with current, on-going star formation (e.g. Magorrian et al. 1998; Kauffmann et al. 2003a; Heckman et al. 2005; von der Linden et al. 2010; Xue et al. 2010; see also Aird et al. 2012). Since AGN require a fuel source (i.e. gas), any physical mechanism that disturbs the morphology of (spiral) galaxies may also directly enhance AGN activity. Alexander & Hickox (2012, and references therein) give a review of how the AGN central engines can grow, such as via direct galaxy mergers. For a mechanism such as galaxy–galaxy harassment (Moore et al. 1996), AGN may trace galaxy interactions and constitute a smoking gun for galaxy evolution (see also Lake, Katz & Moore 1998). The establishment of a link between AGN incidence and environment is still in the balance, however. Whilst some researchers contend that AGN incidence is affected by environment (Kauffmann et al. 2004; Ruderman & Ebeling 2005; Popesso & Biviano 2006; Gilmour et al. 2007; Constantin, Hoyle & Vogeley 2008; Sivakoff et al. 2008; Montero-Dorta et al. 2009; Gavazzi, Savorgnan & Fumagalli 2011) and there may be a ‘Butcher–Oemler AGN effect’ (Eastman et al. 2007; Aird et al. 2012), others come to the opposite conclusion (Miller et al. 2003; Martini, Mulchaey & Kelson 2007; Georgakakis et al. 2008; Sivakoff et al. 2008; Pasquali et al. 2009; Haggard et al. 2010; von der Linden et al. 2010; Atlee et al. 2011).

It is under these considerations that we herein present an analysis of the galaxy population of Abell 1691 based on Sloan Digital Sky Survey (SDSS) data (Abazajian et al. 2009). Abell 1691 is an intermediate X-ray luminosity cluster ($L_X = 0.889 \times 10^{44}$ ergs $^{-1}$; Ebeling et al. 2000; see Jensen & Pimbblet 2012 for an introduction to our intermediate L_X studies) and, as such, may not constitute as extreme an environment as higher X-ray luminosity clusters that have been studied in detail and extensively elsewhere (Pimbblet et al. 2006). For example, Jensen & Pimbblet (2012) find that the modal colour of red-sequence galaxies in intermediate X-ray luminosity clusters at $z \sim 0.08$ is less than for higher X-ray luminosity (i.e. higher mass) galaxy clusters (Pimbblet et al. 2006). The reason for selecting Abell 1691 for a single-case study is that it contains a large number of spectroscopically confirmed redshifts within $3r_{\text{virial}}$ (see Section 3 and Jensen & Pimbblet 2012) and is a relatively understudied cluster in the literature but representative of the intermediate L_X ranges investigated in our previous work (Jensen & Pimbblet 2012).

The data sets that we use in this work are described in Section 2. We begin our analysis of Abell 1691 in Section 3 by determining cluster membership from a gapping approach and searching for any large-scale sub-structuring. In Section 4, we examine how the cluster environment affects AGN cluster members. We complement this with an analysis of the colour–magnitude relation of the cluster in Section 5. In Section 6 we apply a spectroscopic classification scheme to the cluster members to examine the duty cycle of the cluster’s galaxies. This is complemented with an investigation of the environment of red and passive spiral galaxies. In Section 7 we determine how mass drives AGN fraction, blue fraction and spectroscopic duty cycle before summarizing our main conclusions in Section 8.

Throughout this work, we adopt a standard, flat cosmology with $\Omega_M = 0.238$, $\Omega_\Lambda = 0.762$ and $H_0 = 73 \text{ km s}^{-1} \text{ Mpc}^{-1}$ (Spergel et al. 2007).

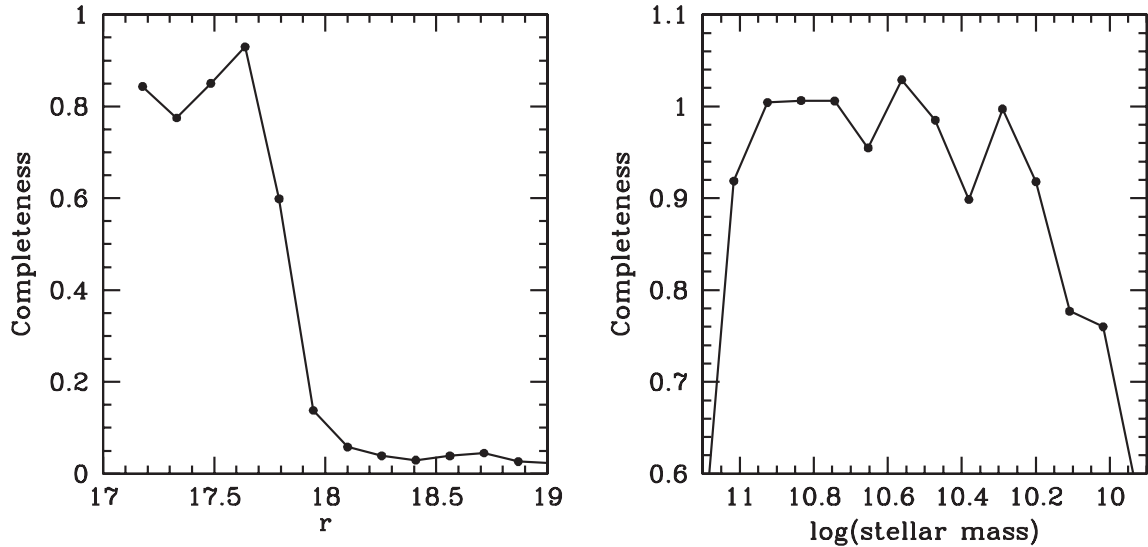


Figure 1. Completeness for our galaxy sample in terms of apparent r -band magnitude (left) and stellar mass (right). At $r = 17.7$ and $\log(\text{stellar mass}) = 10.2$, the data are ~ 90 per cent complete.

2 DATA SET

In this work, we make use of SDSS Data Release 7 (Abazajian et al. 2009). We download all galaxies that have had spectroscopic observations taken within 2° of the nominal cluster centre of Abell 1691 (as specified by the NASA Extragalactic Data base; NED). We note that the SDSS spectroscopy aims to be 100 per cent complete down to a magnitude limit of $r = 17.77$ for all sky areas (Strauss et al. 2002). This magnitude limit corresponds to $\sim M^* + 1$ at the redshift of the cluster. In reality, the $r = 17.77$ target selection may not be 100 per cent spectroscopically complete due to the limitations of how close pairs of spectra can be observed (Blanton et al. 2003). The interlacing of latter spectroscopic observations may recover some of these collision limitations, but the final completeness requires investigation (Fig. 1).

At various points in the subsequent analysis we restrict ourselves to $r = 17.77$ to maximize the number of redshifts we work with and probe down to a mass of $\log(\text{stellar mass}) \approx 10$ (where stellar mass has units of solar masses throughout this work). We evaluate how complete we are at these magnitudes by determining the fraction of spectroscopic targets that are observed by SDSS and generate a successful redshift compared to how many are potentially available for spectroscopic observation in Fig. 1. We find that at $r = 17.77$, we are ~ 90 per cent complete. To evaluate how complete we are in stellar mass for this sample, we construct histograms of stellar mass and fit a log-linear relation to the range $11 < \log(\text{stellar mass}) < 10.5$ (where we anticipate being ~ 100 per cent complete) and extrapolate to lower masses. We find that our catalogue is > 90 per cent complete at $\log(\text{stellar mass}) = 10.2$. We contend that these limits in apparent r -band magnitude and stellar mass are more than satisfactory for the purposes of the present work.

In addition, we marry the data set up with line measurements derived by Tremonti et al. (2004) to provide equivalent width values for important spectral lines that we use in this work and star formation rates from Brinchmann et al. (2004). This is supplemented by morphological data from the Galaxy Zoo project (Lintott et al. 2008, 2011). In brief, Galaxy Zoo is an online ‘citizen science’ undertaking that invites members of the public to morphologically classify SDSS galaxies into several categories. The classifications agree with professional astronomers to an accuracy of better than

90 per cent (Lintott et al. 2008). That said, we caution that the resolution of Galaxy Zoo may cause a blending of some classes (particularly at the Sa/S0 borderline; cf. Andreon & Davoust 1997). Given these caveats and the fact that the Galaxy Zoo morphologies compare well with various external data sets (Lintott et al. 2008), we limit ourselves in this work to dividing our galaxies into three categories: spiral, elliptical and uncertain from Galaxy Zoo.

3 CLUSTER MEMBERSHIP

Cluster membership for Abell 1691 is determined from the SDSS spectroscopy (Fig. 2). There are a number of techniques for defining cluster membership from such data, but one of the most widely used and simplest is a sigma-clipping (or ‘gapping’) approach (Yahil & Vidal 1977; Zabludoff, Huchra & Geller 1990; see also Pimblet et al. 2006). This approach takes the redshift distribution and applies sensibly chosen upper and lower bounds to the region of interest (upper panel of Fig. 2). The mean and standard deviation of these galaxies are then computed. Any galaxy found to be beyond $3\sigma_z$ of the mean is then eliminated from the sample. The process is then iterated.

At $z = 0.06$ and 0.08 there appear gaps in the redshift distribution which we use as our first estimate of the upper and lower bounds for the cluster. Applying the clipping technique, we find that $\bar{cz} = 21257 \pm 54 \text{ km s}^{-1}$ with $\sigma_z = 1009_{-36}^{+40} \text{ km s}^{-1}$ where the errors are obtained from the method of Danese, De Zotti & di Tullio (1980).

However, a closer examination of the redshift distribution (Fig. 2) suggests that there may be a foreground structure at $z \approx 0.066$ which may not be part of the cluster proper. Consequentially, if we choose a new lower bound of $z = 0.0695$, we obtain $\bar{cz} = 21614 \pm 27 \text{ km s}^{-1}$ with $\sigma_z = 402_{-18}^{+21} \text{ km s}^{-1}$. These two approaches clearly result in significantly different values of mean cluster redshift and velocity dispersion. To resolve which value we should adopt, we consider two factors: first, whether the foreground structure is coherent (e.g. an infalling group or sub-cluster) and, secondly, an examination of cluster scaling relationships (Popesso et al. 2005).

For the first consideration, we create a map of RA versus Dec. (Fig. 3) and examine it for any structure in redshift bands suggested to us by Fig. 2. This suggests that the foreground redshift peak is

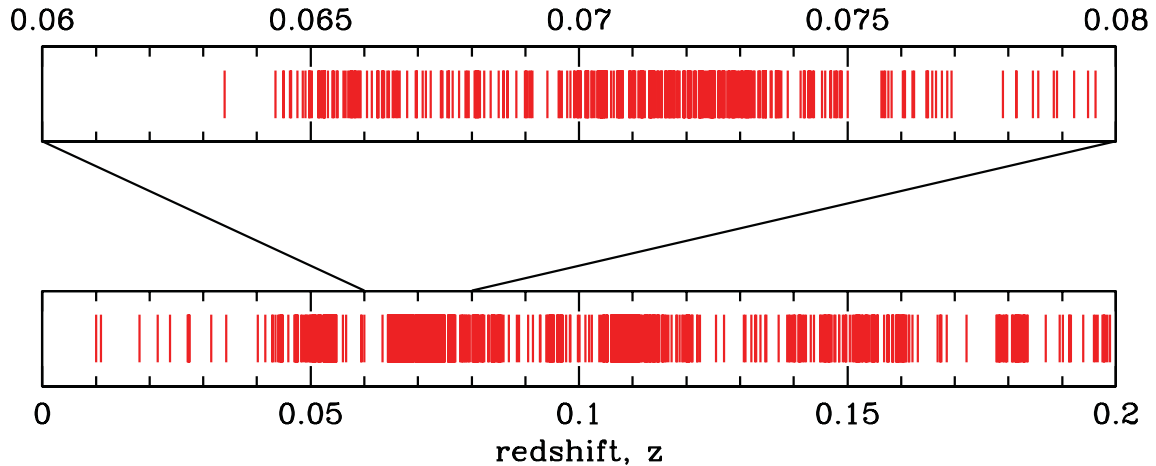


Figure 2. Barcode-style redshift diagram for all galaxies within 2° of Abell 1691. Each vertical line represents an individual galaxy. In the upper plot, we show a zoom-in on the $0.06 < z < 0.08$ region of the lower plot. We use this plot to estimate the upper and lower bounds of the cluster in order to derive its mean redshift and velocity dispersion.

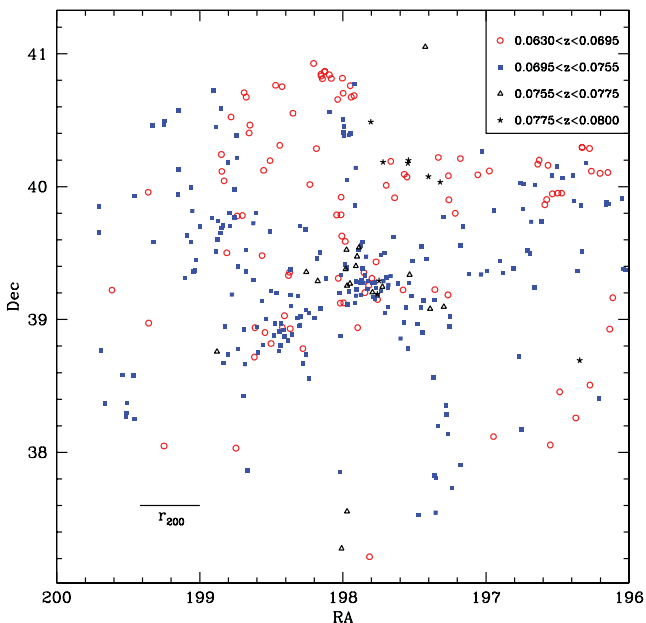


Figure 3. Spatial distribution of all galaxies in our sample with $0.063 < z < 0.080$, coded according to their redshifts. We use this information to derive values for the cluster’s velocity dispersion in conjunction with the redshift distribution and knowledge of L_X . A scale bar showing r_{200} ($= 2.01$ Mpc) at the redshift of the cluster is depicted in the lower-left corner. Several filaments can be seen extending from the centre of Abell 1691 and are presumably fuelling the growth of this cluster (cf. Pimblet, Drinkwater & Hawkrigg 2004).

smearred over the sky and does not represent a group or cluster in its own right (in contrast with Abell 1691 itself which is revealed as a strong overdensity in the centre of this plot, with a significant secondary peak eastwards of the centre and filaments radiating outwards).

For the second consideration, we note that the X-ray luminosity of A1691 is $L_X = 0.889 \times 10^{44}$ ergs $^{-1}$ in the *ROSAT* 0.1–2.4 keV band (Ebeling et al. 2000). Popesso et al. (2005) note that $\log_{10}(L_X) = 3.68 \log_{10}(\sigma_z) - 10.53$ for all galaxies in a given cluster (i.e. not just red early-types). When we plug in our two values for σ_z into the above equation, it yields $L_X = 3.3 \times 10^{44}$ ergs $^{-1}$ for $\sigma_z =$

1009 km s $^{-1}$, and $L_X = 0.1 \times 10^{44}$ ergs $^{-1}$ for $\sigma_z = 402$ km s $^{-1}$. Interestingly, the measured value for L_X lies between these two values. To resolve this, we note that Popesso et al. (2005) quote the 95 per cent confidence level on the scatter of the intercept of this relationship as 0.80. This generates a 95 per cent confidence interval of $0.02 \times 10^{44} < L_X < 0.7 \times 10^{44}$ ergs $^{-1}$ for $\sigma_z = 402$ km s $^{-1}$ and $0.5 \times 10^{44} < L_X < 20.9 \times 10^{44}$ ergs $^{-1}$ for $\sigma_z = 1009$ km s $^{-1}$. This, coupled with Fig. 3, suggests to us that the better redshift interval to derive the cluster parameters from is $0.06 < z < 0.08$ and therefore we adopt $\bar{v}_z = 21257 \pm 54$ km s $^{-1}$ and $\sigma_z = 1009^{+40}_{-36}$ km s $^{-1}$ for Abell 1691.

To check these findings, we finally construct a phase-space diagram (Fig. 4) of velocity versus distance from the centre of the cluster for all galaxies in our magnitude-limited sample using the cluster mass model of Carlberg, Yee & Ellingson (1997). In this, we see that the foreground structure noted above ($0.06 < z < 0.0695$) mixes with the higher redshift range ($0.0695 < z < 0.0755$) at most radii from the cluster centre and, moreover, is well contained within the 3σ caustic contour from the Carlberg et al. (1997) mass model. We therefore adopt our final definition of cluster members as being those galaxies contained within these 3σ limits. This yields a total of 342 galaxies for our study.

3.1 Sub-structure

Although the cluster appears moderately smooth (with a moderate secondary overdensity eastwards of the centre; Fig. 3), we aim to ascertain if there is bona fide sub-structure contained within it. We first turn to *ROSAT* X-ray imaging of the galaxy cluster (Fig. 5) to check if the cluster is experiencing any overt signs of recent interactions (cf. Oemler et al. 2009; Owers, Couch & Nulsen 2009). The lack of sub-structure, coupled with regular (i.e. roughly circular), contours indicates that Abell 1691 is a virialized system that has not had any recent perturbation from (e.g.) an infalling system of comparable mass. But would we be able to detect sub-structure in this X-ray image? First, we note that spatial resolution of *ROSAT* Position Sensitive Proportional Counter is ~ 25 arcsec at 0.93 keV which translates to ~ 33 kpc at the redshift of A1691. This is approximately the diameter of a single galaxy; hence we believe that *ROSAT* has sufficient spatial resolution to resolve sub-structures at the redshift of A1691. Secondly, although there is scatter in the

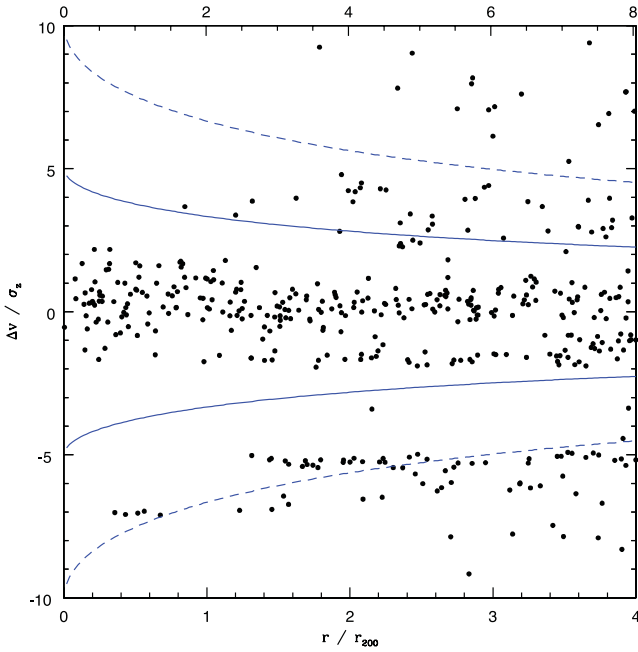


Figure 4. Phase-space diagram of velocity offset as a function of distance from the cluster centre for the galaxies in our sample. The solid lines denote 3σ caustic from the mass model of Carlberg et al. (1997) and the dashed lines are the 6σ caustic. Galaxies inside the solid line are considered cluster members whilst those between the solid and dashed lines can be thought of as infalling.

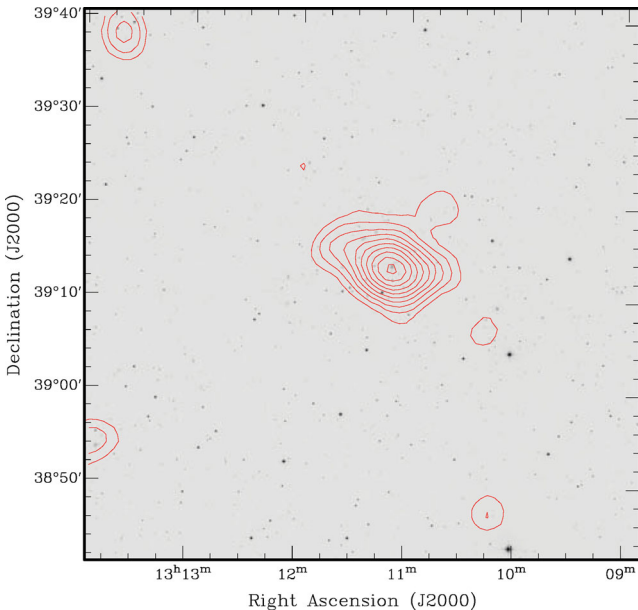


Figure 5. X-ray contour map generated from *ROSAT* 0.1–2.4 keV imaging overlaid on the *r*-band image of Abell 1691. This suggests a cluster core region without significant sub-structure.

L_X –mass relationship (Popesso et al. 2005), we note from fig. 1 of Jensen & Pimblet (2012) that we would be able to detect clusters down to $L_X \sim 0.7 \times 10^{-44}$ ergs $^{-1}$ from *ROSAT*. We explicitly note that that does not preclude a cluster of equal mass being present in our sample, but we regard it as unlikely.

To address this question of sub-structure further, we apply the Dressler & Shectman (1988; DS) sub-structure test to our data set.

This test is the most sensitive available to detect sub-structure in the literature (Pinkney et al. 1996). It works by calculating the mean local velocity (\overline{cz}) and local velocity standard deviation (σ_{local}) of given galaxies N nearest neighbours (where N is chosen to be the 10 nearest neighbours). To determine if there exists significant sub-clustering, these values are compared to the parent cluster’s mean velocity and σ_z such that

$$\delta^2 = \left(\frac{N_{\text{local}} + 1}{\sigma_v^2} \right) \left[(\overline{cz}_{\text{local}} - \overline{cz})^2 + (\sigma_{\text{local}} - \sigma_v)^2 \right] \quad (1)$$

where δ is a measure of the deviation of the individual galaxy. The parameter of merit, Δ , is then the summation of all δ terms in the cluster. This is compared to a Monte Carlo re-simulation of the cluster wherein the velocities are randomly re-assigned to each galaxy to generate $P(\Delta)$ and thereby estimate the confidence level that the cluster contains sub-structure. For Abell 1691, we find that $P(\Delta) < 0.01$, suggesting that it has significant sub-structuring. This can be seen in Fig. 6 where we plot circles on the basis of a galaxies’ e^δ value – overlapping large circles in close proximity are therefore logically interpreted as sub-structure (see DS).

Although the cluster core ($r < \sim 0.5$) is largely free of sub-clustering, we see that there is a significant grouping to the north of the main cluster overdensity (RA ≈ 198 , Dec. ≈ 40.8). We perform a search of the NED to attempt to identify this. The best match is cluster entry number 632 from Yoon et al. (2008; redshift $z = 0.0677$, at $0.95\sigma_z$ from the mean redshift of Abell 1691). This group is therefore probably a minor infalling group to Abell 1691 that has been picked up by the DS algorithm.

Also apparent from Figs 3 and 6 are several (arguably three or four) filaments that link to the core of Abell 1691 – particularly the eastern extension of the cluster core. Given the velocity dispersion of the cluster, it is not unexpected to see these many filaments connecting to it (Pimblet et al. 2004).

4 AGN

We now turn to the active galaxy population. To determine which cluster members are AGN, we make use of a BPT diagram (Baldwin, Phillips & Terlevich 1981). By plotting flux ratio $[\text{O III}]/\text{H}\beta$ against $[\text{N II}]/\text{H}\alpha$, Baldwin et al. (1981) are able to effectively separate AGN from star-forming galaxies. Implicitly, the use of the BPT diagram means that we are identifying type 2 AGN (those AGN that are obscured by a dusty circumstellar medium and give rise to strong narrow emission lines) rather than type 1 AGN (a direct view of the broad-line region). We check this is true by confirming that all galaxies classed as AGN by the BPT diagram have an SDSS spectroscopic classification of ‘galaxy’ (as opposed to ‘QSO’).

In Fig. 7 we show the BPT diagram for our cluster members that have signal-to-noise ratio (S/N) > 3 in the requisite lines. To split the AGN from star-forming galaxies, we use the Kauffmann et al. (2003a; see also Veilleux & Osterbrock 1987; Kewley et al. 2001; Brinchmann et al. 2004; Stasińska et al. 2006) relation for AGN: $\log_{10}([\text{O III}]/\text{H}\beta) > 0.61 / \{\log_{10}([\text{N II}]/\text{H}\alpha) - 0.05\} + 1.3$. Although we could extend our analysis to weaker AGN classes and ‘retired’ AGN (Cid Fernandes et al. 2010), we elect to stick to the Kauffmann et al. approach due to its wider adoption in the literature. We also draw on the definitions of Seyferts and low-ionization nuclear emission-line regions (LINERs) (see Kauffmann et al. 2003a; Ho, Filippenko & Sargent 1997). Our BPT diagram is typical of the general galaxy population, including a LINER galaxy with an elliptical morphology (cf. Heckman 1980). A visual check

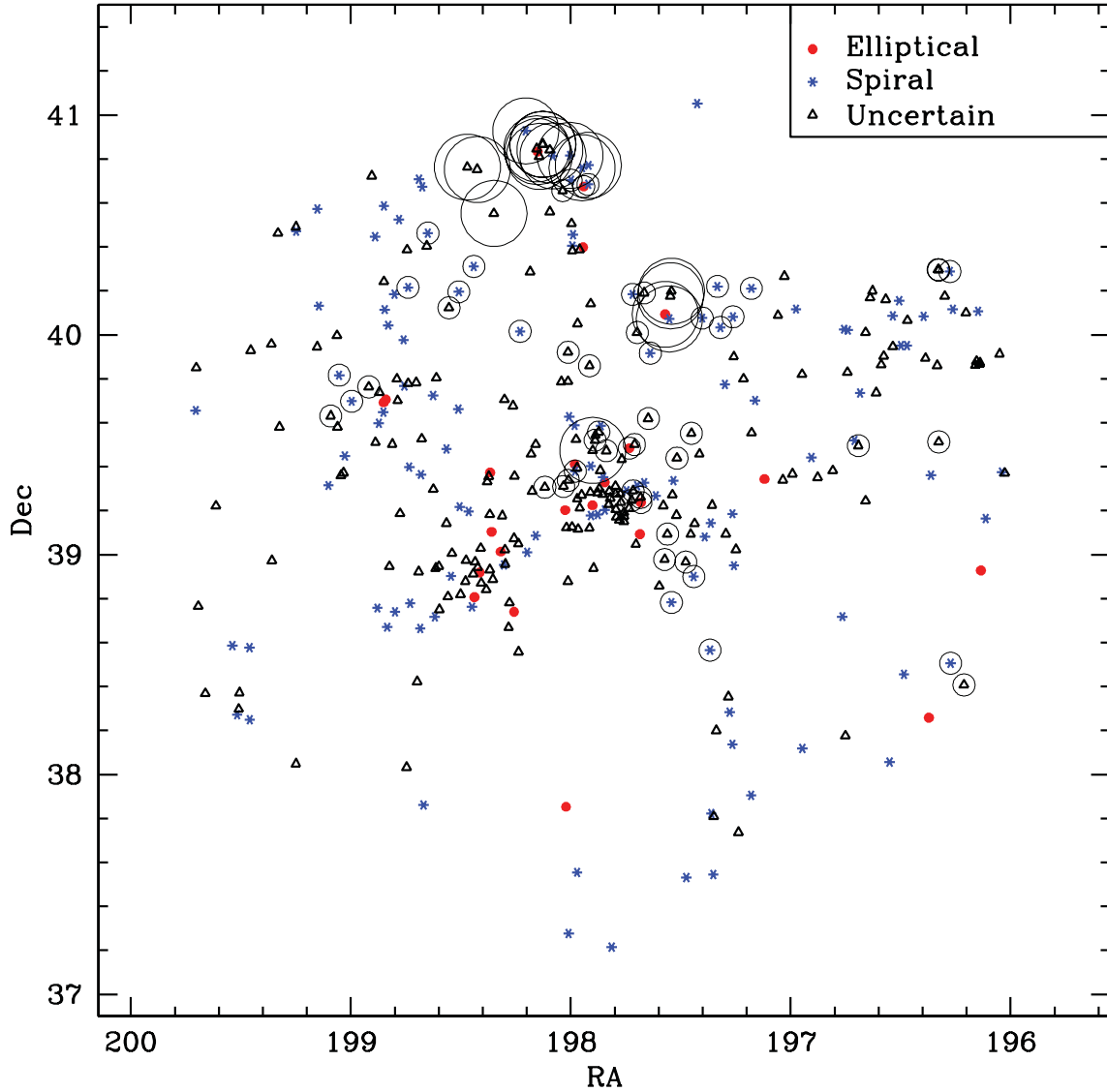


Figure 6. DS test result with galaxy members coded according to their Galaxy Zoo morphologies (ellipticals are red circles; spirals are blue stars; uncertain morphologies are open black triangles). Normally, one would plot circles around each point that have a radius proportional to e^δ . However, to improve clarity, we only plot two circle radii to denote modest and significant values of e^δ (smaller and larger circles, respectively). Sub-structure is interpreted as overlapping circles in close proximity. The main clump of sub-structure is seen to be north of the central overdensity (RA \approx 198, Dec. \approx 40.8) and may be an infalling group.

of the SDSS imaging confirms the Galaxy Zoo morphology class: this galaxy is indeed an early-type (possibly S0).

Is the number of AGN that we find in Abell 1691 typical? To address this question, we note that Popesso & Biviano (2006) make a study of several hundred galaxy clusters and find that the fraction of AGN anti-correlates with σ_z . Explicitly, they report that $f_{\text{AGN}} = (-1.21 \pm 0.12)\log(\sigma_z) + (2.50 \pm 0.24)$ (Popesso & Biviano 2006). This equation predicts an AGN fraction of 0.07 for A1691 using $\sigma_z = 1009 \text{ km s}^{-1}$, and 0.22 using $\sigma_z = 402 \text{ km s}^{-1}$ (see above for the derivation of these two values of σ_z). We note their definition of the fraction of AGN contained in a cluster is the number of AGN divided by the total galaxy population within r_{200} and brighter than $M_r = -20.0$. We compute r_{200} from Girardi et al. (1998): $r_{200} \sim r_{\text{virial}} = 0.002\sigma_z = 2.01 \text{ Mpc}$. At the mean redshift of Abell 1691, this radius corresponds to 25 arcmin. For convenience (and to be in-line with the calculation of f_B , below) we stick to our magnitude limit of $r = 17.77$. We obtain $f_{\text{AGN}} = 5/75 = 0.06 \pm 0.03$ (where the

quoted error is simply a Poissonian error). This fraction is consistent with the (anti-correlation) equation reported by Popesso & Biviano (2006; see above) that predicts $f_{\text{AGN}} = 0.07$ for our cluster if we adopt $\sigma_z = 1009 \text{ km s}^{-1}$, and is more than 3σ away from the AGN fraction predicted for $\sigma_z = 402 \text{ km s}^{-1}$. Therefore this firms our above argument that $\sigma_z = 1009 \text{ km s}^{-1}$ is the correct velocity dispersion for the cluster.

5 COLOUR-MAGNITUDE RELATION

On a colour-magnitude plane, a galaxy cluster exhibits a strong correlation for its early-type members: the so-called red sequence (e.g. Visvanathan & Sandage 1977; Bower, Lucey & Ellis 1992). Fig. 8 displays the r versus $(g-r)$ colour-magnitude diagram for cluster members within r_{200} of the cluster centre. We fit the red sequence as per Jensen & Pimblet (2012), using the Lorentzian merit function minimized using the Nelder-Mead down-hill simplex algorithm

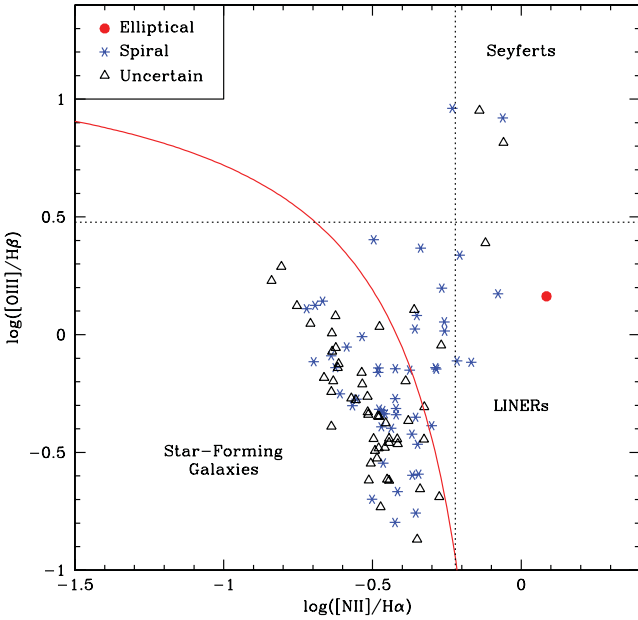


Figure 7. BPT diagram for all cluster members with $S/N > 3$ in each line. The Kauffmann et al. (2003a) division between AGN and star-forming galaxies is the solid curve, and we also mark the loci of Seyferts ($[\text{O III}]/\text{H}\beta > 3$ and $[\text{N II}]/\text{H}\alpha > 0.6$) and LINERs ($[\text{O III}]/\text{H}\beta < 3$ and $[\text{N II}]/\text{H}\alpha > 0.6$) with the vertical and horizontal dotted lines. The point types correspond to the Galaxy Zoo morphological classifications of these galaxies.

(Press et al. 1992). The scatter in the intercept of the red-sequence fit is displayed as parallel lines around the red-sequence fit in Fig. 8, along with the Galaxy Zoo morphology classifications and identified AGN.

We use Fig. 8 to define the blue fraction (f_B) of galaxy cluster members in an analogous way to Butcher & Oemler (1984). Formally, Butcher & Oemler defined f_B to be the fraction of galaxies that are brighter than $M_V = -20$ and have a rest-frame colour that is 0.2 in $(B - V)$ bluer than the fitted colour-magnitude relation. However, since we are only interested in comparing relative values (rather than comparing f_B to external works), we simplify this definition for our convenience by defining f_B to be those galaxies 0.2 in $(g - r)$ bluer than the fitted red sequence as our definition of blue. For the magnitude limit, we convert $M_V = -20$ to r band using one of the stellar magnitude conversions presented in Jester et al. (2005): $V = g - 0.59 \times (g - r) - 0.01$ and assuming a ‘typical’ colour for our galaxies (namely the red-sequence colour at M^*). This gives a limit of $r \approx 18.3$. This is fainter than our r -band selection limit for our sample and we therefore use all galaxies in our sample for f_B calculations, below. Additionally, we note that this is an invalid conversion since we have not used point sources and made assumptions about the typical galaxy colour. We re-emphasize that we are only interested in the relative trend within our own data set rather than an absolute comparison to external data sets and therefore our approach is sound for this purpose.

In Fig. 9 we plot the variation of f_B , by our definition, with radius from the cluster centre. We complement this trend with the radial variation of f_{AGN} (as defined in Section 4). The trend in f_B is to increase away from the cluster core, but for f_{AGN} , it looks reasonably flat until a very high radius from the cluster centre; and even there the f_{AGN} trend is not significant. The best statement we can make is that the cluster core appears hostile to both bright blue galaxies and active galaxy types.

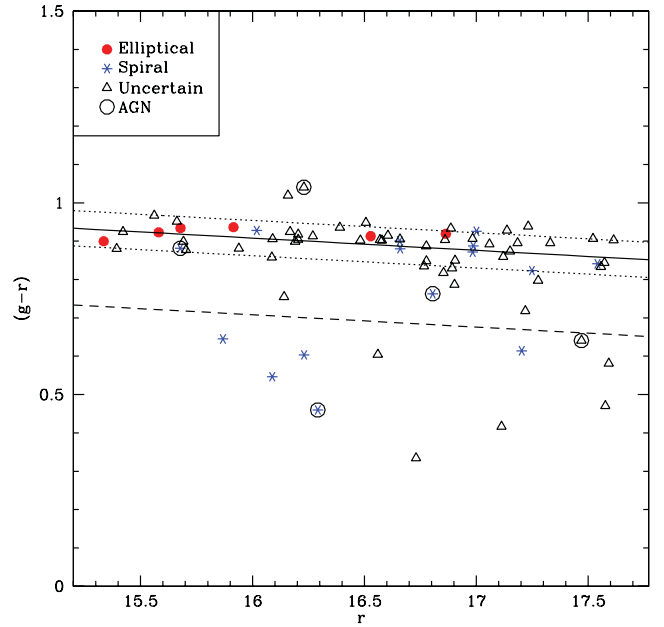


Figure 8. Colour-magnitude relation for cluster members within r_{200} of the cluster centre. Symbols are the same as for the BPT diagram (Fig. 7), and we circle our identified AGN. The solid line displays the fit to the red sequence with the scatter in the fit’s intercept denoted by the parallel dotted lines. The dashed lines denote the limits used to define f_B (i.e. blue galaxies are to the left and below these lines).

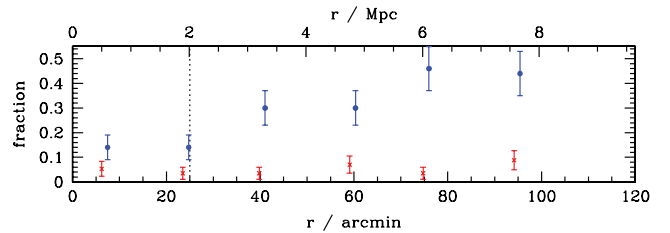


Figure 9. Radial variation of the blue fraction, f_B (blue circles), and the AGN fraction, f_{AGN} (red crosses), in Abell 1691. The vertical dotted line denotes r_{virial} and each point contains the same number of galaxies (with f_B arbitrarily offset slightly from f_{AGN} for the sake of clarity). The two different fractions follow the same (weak) trend to an approximation – the cluster core being hostile to both blue galaxies and AGN.

Many other authors have previously noted the lack of bright blue galaxies in the cores of clusters and the (weak) radial trend for f_B (Kodama & Bower 2001; Dahln, Fransson & Nslund 2002; Dahln et al. 2004; Tran et al. 2005; Li, Yee & Ellingson 2009; Raichoor & Andreon 2012a; see also Chung et al. 2011, who note that ‘the fraction of star-forming galaxies increases with cluster radius but remains below the field value even at $3r_{200}$ ’) for a given absolute magnitude limit used to define the Butcher–Oemler effect. Our results for Abell 1691 support these previous works and add weight to the arguments presented elsewhere (Wilman, Zibetti & Budavari 2010; Hou et al. 2012; Wetzel, Tinker & Conroy 2012) that the red galaxy fraction (i.e. $1 - f_B$) correlates with environment only up to ~ 1 Mpc away from the cluster core. A tantalizing facet of Fig. 9 is the upturn of f_B at 2–3 Mpc from the cluster core. Although statistically not significant, we note that this radius is about the same seen by Porter et al. (2008) who report a fractional enhancement in starbursting galaxies at these radii along filaments of galaxies. We therefore hypothesize that this maximum is a reflection of this

enhanced star formation rate seen by Porter et al. (2008) and probably caused by first-time harassment (Moore et al. 1996) of galaxies within those filaments. A much larger sample of galaxy clusters will be required to probe this blue fraction enhancement and definitively ascertain whether such an enhancement is significant.

The radial variation for f_{AGN} has also been noted by other authors (Johnson, Best & Almaini 2003; Kauffmann et al. 2003a; Gilmour et al. 2007; Hwang et al. 2012), but there are yet others who suggest that the AGN distribution may be flat (as we find out to several Mpc), or even concentrated towards the cluster centres (Ruderman & Ebeling 2005; Branchesi et al. 2007; Martini et al. 2007). Our results support a mild increase in AGN fraction at large radii away from the cluster centre, but otherwise suggest a flat distribution. This result supports the notion that AGN incidence may be driven by galaxy–galaxy interactions when there is an available gas supply to fuel the AGNs.

6 SPECTROSCOPIC CLASSIFICATION

We further quantify the galaxy population by classifying the cluster members on the basis of the line strengths of two key diagnostic features: H δ and [O II] (Dressler et al. 1997; Poggianti et al. 1999; see also Pimblet et al. 2006). In combination, these two lines can successfully discriminate between a number of important stages in galaxy evolution, including the E+A phase (i.e. strong H δ absorption coupled with a lack of current star formation as indicated by a lack of [O II] emission). Although we could have used H α as our indicator of present star formation, we elect to employ this classification scheme to be in-line with previous studies. A summary of the classification scheme along with its broad interpretations is presented in Table 1.

In Fig. 10 we display the spectroscopic classifications of cluster members split by radial bin from the cluster core. As would be expected, the passive k-type galaxies dominate at the cluster core (Table 2) and gradually fall-off with increasing radius away from the cluster centre (indeed, the outermost radial bin may be regarded as the ‘field’ value). The values for the total emission classes versus non-emission classes are very comparable to the values reported by Pimblet et al. (2006) for massive, highly X-ray luminous clusters (a non-emission class fraction of 0.82 within r_{200} and 0.74 beyond r_{200}) which are in turn a higher fraction than high-redshift massive clusters (Poggianti et al. 1999).

6.1 Red and passive spirals

Figs 8 and 10 contain a number of spiral galaxies that are red and (or) passive. Since spiral galaxies possess young stellar populations, the existence of these red spiral galaxies is potentially, at first glance, surprising. However, the colour of a galaxy and its morphology are likely to be driven by different mechanisms: the colour is a reflection of the recent star formation history (say, within the past \sim Gyr) whilst the morphology is more sensitive to recent kinematic or dynamical events in the galaxies’ life (cf. Boselli & Gavazzi 2006). Red and passive spiral galaxies within clusters may therefore represent an important, but brief, transition phase in the life of a galaxy: a point at which its star formation rate has been truncated (or all the star-forming gas has been used up) but it is yet to undergo significant morphological transformation to an S0 or elliptical morphology (Goto et al. 2003b; Moran et al. 2006; Wolf et al. 2009; Bundy et al. 2010; Lee et al. 2010; Masters et al. 2010; see also Ishigaki, Goto & Matsuhara 2007; Mahajan & Raychaudhury 2009).

To investigate the relation of red, passive spiral galaxies with environment, we now extract them from our catalogue using the following criteria: (i) they must be of the ‘k’ spectroscopic class (Table 1); (ii) they must be spiral as defined by Galaxy Zoo; (iii) they must be photometrically red – within the dotted parallel lines that represent the scatter of the colour–magnitude relation’s fitted intercept displayed on Fig. 8. This yields 18 red and passive spiral galaxy cluster members within $4r_{200}$. Within r_{200} , 5/15 spiral galaxies are red and passive (0.33 ± 0.15). This changes to 13/81 (0.16 ± 0.05) between r_{200} and $4r_{200}$. Expressed as a fraction of the total cluster population, the red and passive spiral galaxies constitute a fraction of ~ 0.06 at all radii. This suggests a lack of significant environmental dependence for the location of red and passive spiral galaxies and agrees with Masters et al. (2010) who note that although red spirals may prefer intermediate environs, ‘environment alone is not sufficient to determine if a galaxy will become a red spiral’. Gallazzi et al. (2009) argue that red star-forming galaxies seem ubiquitous at all galaxy densities. Given the relationship between radius and density for cluster galaxies, this supports our result of a none varying fraction of red passive spirals with radius. This means that an environmental mechanism such as harassment may not be required to explain such galaxies: a quenching event followed by a slow morphological transformation is likely to be sufficient to cause these observations (Wolf et al. 2009). This supports Bamford et al. (2009) who argue that the time-scale for morphological transform is longer than that for colour transform on the basis of an environmental dependence with galaxy colour at a fixed morphology from Galaxy Zoo (Lintott et al. 2008).

7 MASS RELATIONSHIPS

The above analysis has considered the relationship between various parameters, such as AGN fraction, to environment – proxied as the distance from the cluster centre.¹ To better explore the covariance of environment and galaxy mass, we now re-do the above analysis but use galaxy stellar mass as our primary abscissa. We obtain the galaxy stellar mass for our cluster members from the SDSS value-added catalogue (see www.mpa-garching.mpg.de/SDSS/DR7/Data/stellarmass.html). Although the original stellar mass estimates by Kauffmann et al. (2003b) are based on the EW of H δ and the D4000 Å break, the data used here are based on the fit to the SDSS photometry which, like Kauffmann et al. (2003b), uses a large set of Bruzual & Charlot (2003) models to derive its output. The distributors of the data set note that there are some differences to the line index fit derived stellar masses of Kauffmann et al. (2003b), including better accuracy at lower masses (see www.mpa-garching.mpg.de/SDSS/DR7/mass_comp.html). We therefore contend that these masses should be more than robust enough for our purposes of correlating AGN fraction (etc.) with mass.

Before we repeat the above analysis for f_{AGN} and f_{B} using galaxy stellar mass (as above), we must guard against the selection bias of having a top-end mass limit with a low-end r -band magnitude limit (cf. Holden et al. 2007). We therefore construct a mass versus absolute magnitude diagram and find the mass limit at which we are complete for the reddest galaxies (i.e. colour–magnitude red-sequence galaxies) and the absolute magnitude limit corresponding

¹ Distance to the cluster centre can also be considered a temporal measure, i.e. the time since infall (Gao et al. 2004), but such a signal may be contaminated (e.g. Pimblet 2011).

Table 1. Spectroscopic classification scheme used in this work and its broad interpretation (see Poggianti et al. 1999; see also Poggianti, Bressan & Franceschini 2001). A further class of a+k is noted by Poggianti et al. (1999) but we do not use it here as we have no galaxies that would be classified as an a+k type.

Class	Definition	Interpretation
k	$EW(H\delta) < 3 \text{ \AA}$ and $EW([O II]) > -5 \text{ \AA}$	Passive: star formation ceased approximately several Gyr ago.
k+a	$EW(H\delta) > 3 \text{ \AA}$ and $EW([O II]) > -5 \text{ \AA}$	Post-starburst: a young population of A-stars with no present star formation.
e(c)	$EW(H\delta) < 4 \text{ \AA}$ and $-5 > EW([O II]) > -40 \text{ \AA}$	Star-forming galaxy; similar to a present-day, steadily star-forming, spiral galaxy.
e(a)	$EW(H\delta) > 4 \text{ \AA}$ and $-5 > EW([O II]) > -40 \text{ \AA}$	Recent, strong starburst galaxy whose star formation rate is falling back down.
e(b)	$EW([O II]) < -40 \text{ \AA}$	On-going starburst.

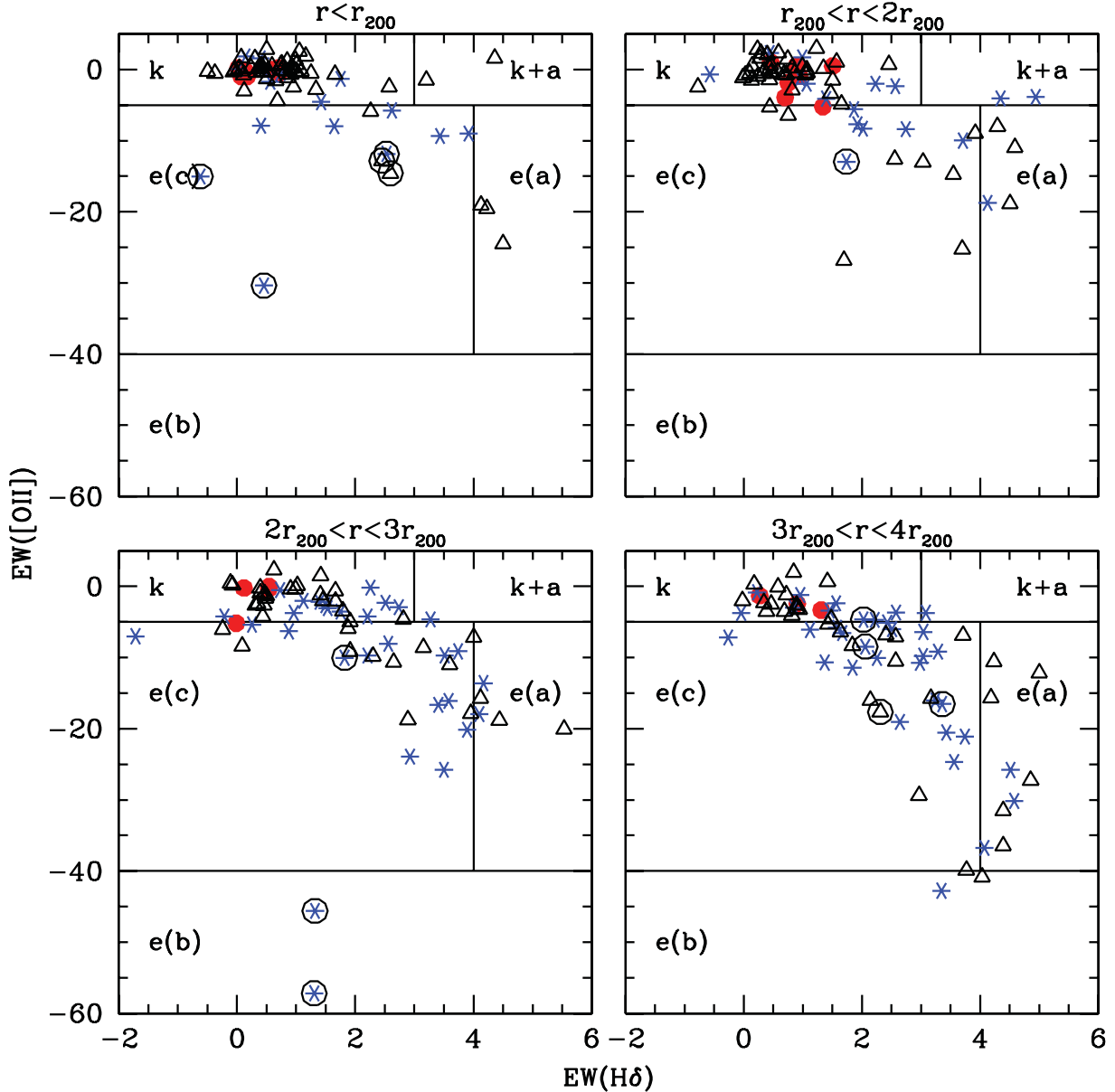


Figure 10. Spectroscopic classifications of the cluster galaxy population according to the Poggianti et al. (1999) scheme which is based on EW measurements of H δ and [O II] and which we split by radius from the cluster centre. By convention, emission lines are reported with negative values. Morphological types from Galaxy Zoo are marked with different symbols and AGN are circled (as per Fig. 8).

to $r = 17.77$ at the mean cluster redshift (Fig. 11). These limits are $\log(\text{stellar mass}) = 10.2$ and $M_R = -19.55$, respectively, and we only use galaxies more massive and brighter than these limits (Fig. 11) in the subsequent analysis. This ensures that we will

be complete for these galaxies, regardless of the star formation history.

The results are displayed in Fig. 12. There are two striking features about this plot. First the blue fraction, f_B , appears to be

Table 2. Radial fractions of different spectroscopic classes. The final two rows give the summed emission class fractions [e(b) plus e(a) plus e(c)] and non-emission class fractions (k plus k+a classes). All errors are Poisson.

Class	$r < r_{200}$	$r_{200} < r < 2r_{200}$	$2r_{200} < r < 3r_{200}$	$3r_{200} < r < 4r_{200}$
k	0.80 ± 0.10	0.70 ± 0.10	0.54 ± 0.10	0.39 ± 0.07
k+a	0.03 ± 0.02	0.03 ± 0.02	0.01 ± 0.01	0.01 ± 0.01
e(c)	0.14 ± 0.04	0.21 ± 0.05	0.33 ± 0.07	0.45 ± 0.08
e(a)	0.04 ± 0.02	0.05 ± 0.03	0.09 ± 0.03	0.13 ± 0.04
e(b)	Nil	Nil	0.03 ± 0.02	0.03 ± 0.02
Emission classes	0.18 ± 0.06	0.26 ± 0.06	0.45 ± 0.08	0.61 ± 0.07
Non-emission classes	0.83 ± 0.11	0.73 ± 0.11	0.55 ± 0.10	0.40 ± 0.10

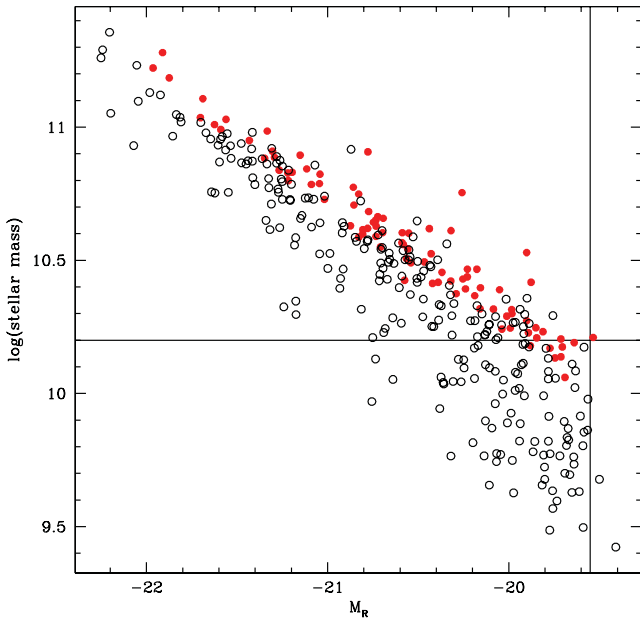


Figure 11. Galaxy mass versus absolute magnitude for cluster members. The red filled circles are the red-sequence galaxies. The horizontal line denotes the mass limit at which we are complete for the reddest galaxies (i.e. red-sequence galaxies, or redder, as defined by the scatter around the line of best fit in Fig. 8), whilst the vertical line is $r = 17.77$ at the mean cluster redshift. We avoid biasing our mass relation analyses by using only galaxies in the upper left (high-mass, brighter) quadrant of this plot.

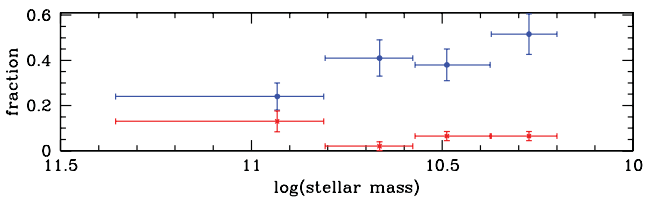


Figure 12. As for Fig. 9, but the blue fraction (blue circles) and AGN fraction (red crosses) are plotted as a function of galaxy stellar mass. The errors in the y-direction are Poissonian. However, the ‘errors’ in the x-direction simply denote the full range of galaxy stellar mass that each point is derived from. The blue fraction is driven by low-mass galaxies ($\sim 3\sigma$ level) whereas the AGN fraction appears mostly driven by high-mass galaxies ($\sim 2\sigma$ level).

primarily driven by low stellar mass galaxies [$\log(\text{stellar mass}) < 10.8$]. The difference between the lowest mass bin and the highest is significant at an $\sim 3\sigma$ level for f_B . Although the trend in AGN fraction suggests that f_{AGN} is being driven by the higher mass

regimes in agreement with previous works (Brusa et al. 2009; Xue et al. 2010) and unsurprising given that supermassive black holes are almost exclusively found in massive galaxies (Magorrian et al. 1998), our limited sample is only able to place a significance of $\sim 2\sigma$ on this trend. In both cases, these trends are much stronger than found in Fig. 9. The inference of this result for the Butcher–Oemler effect is that it is almost exclusively driven by lower mass [$\log(\text{stellar mass}) < 10.8$] galaxies. This is supported by Tajiri & Kamaya (2001) who contend that blue Butcher–Oemler galaxies are the less massive cluster galaxies that also possess small (cluster frame) peculiar velocities and De Propris et al. (2003) who note that the Butcher–Oemler effect is primarily due to low-luminosity galaxies that are presently star forming.

In Table 3 we compute the spectroscopic classifications for our galaxies (as per Table 2), but split on galaxy mass using the bias-corrected sample (Fig. 11). Immediately we see that the passive k types are dominant at the high-mass regime [$\log(\text{stellar mass}) > 10.5$]. This supports the notion that massive galaxies are mostly non-star-forming and dead, regardless of their environment. Meanwhile, of the emission line classes, the recent starburst galaxies [e(a) types; but also see Poggianti et al. 2001, who suggest the e(a) class may include a significant contribution from on-going dust-enshrouded starbursts] are exclusively found at lower mass regimes.

We now turn to the red and passive spiral galaxies in the bias-corrected sample. Out of all spiral galaxies, we find that 6/37 (0.16 ± 0.07) are red and passive at $\log(\text{stellar mass}) < 10.5$, whereas this grows to 12/48 (0.25 ± 0.07) at $\log(\text{stellar mass}) > 10.5$. In terms of the whole galaxy population, these fractions become 0.06 ± 0.01 and 0.08 ± 0.02 , respectively (where the errors are Poissonian). Although not highly significant (i.e. less than 2σ difference), this provides the tantalizing suggestion that the red and passive population is driven by higher mass rather than environment. This agrees with observations made by Masters et al. (2010) who show that red galaxies are predominantly massive galaxies, regardless of their morphology. Since Galaxy Zoo is limited to simply saying that a given galaxy is a spiral, hence a future line of investigation would be to determine the sub-class of spiral that these red and passive spirals are. We could then address whether earlier spiral (i.e. Sa) classes dominate the passive spiral fraction.

7.1 Velocity dispersion profiles

Pimblet et al. (2006) note that the velocity dispersion of different spectroscopic classifications of galaxies can vary strongly – the emission line galaxies tending to yield larger velocity dispersions at higher radii from the cluster centre. This ties into work decades earlier by (e.g.) Rood et al. (1972) who note different profiles for red and blue galaxies. However, Pimblet et al. make no comment about

Table 3. As for Table 2, but for stellar mass fractions of the different spectroscopic classes.

Class	$11.5 > \log(\text{stellar mass}) > 10.8$	$10.8 > \log(\text{stellar mass}) > 10.5$	$10.5 > \log(\text{stellar mass}) > 10.2$
k	0.79 ± 0.11	0.82 ± 0.10	0.62 ± 0.08
k+a	Nil	0.04 ± 0.02	0.01 ± 0.01
e(c)	0.17 ± 0.05	0.14 ± 0.04	0.33 ± 0.06
e(a)	Nil	Nil	0.04 ± 0.02
e(b)	0.03 ± 0.02	Nil	Nil
Emission classes	0.20 ± 0.05	0.14 ± 0.04	0.37 ± 0.06
Non-emission classes	0.79 ± 0.11	0.86 ± 0.10	0.63 ± 0.08

how galaxy mass may affect these profiles. Here, we compute the velocity dispersion profile [$\sigma_p(R)$] by mass for A1691 by following a method originally detailed by Bergond et al. (2006) for use with globular cluster systems that has since found adoption in application to galaxy clusters (Hou et al. 2009, 2012).

The method involves the use of a moving window (or kernel) that takes into account the redshift measurements of all cluster members for each radial bin rather than simply using binned radii. The projected velocity dispersion profile is defined as

$$\sigma_p(R) = \sqrt{\frac{\sum_i w_i(R)(x_i - \bar{x})^2}{\sum_i w_i(R)}} \quad (2)$$

where R is the radius from the centre of the cluster, x_i are the measured redshifts (or radial velocities), \bar{x} is the mean redshift of the cluster (as determined above) and w_i is the weighting function such that:

$$w_i(R) = \frac{1}{\sigma_R} \exp\left(-\frac{(R - R_i)^2}{2\sigma_R^2}\right) \quad (3)$$

where σ_R is the chosen width of the window (here, set to a constant value of 30 arcmin).

The resultant velocity dispersion profiles for high-mass [$\log(\text{stellar mass}) > 10.7$], low-mass [$\log(\text{stellar mass}) < 10.5$]

and all cluster galaxies for our bias-corrected sample is displayed in Fig. 13. To obtain uncertainties on these profiles, we take a Monte Carlo approach and bootstrap our samples 1000 times. The error bounds depicted in Fig. 13 are the 1σ standard deviations from these 1000 Monte Carlo trials.

To interpret Fig. 13, we note that a rising profile would be indicative of interacting systems (cf. Menci & Fusco-Femiano 1996; Hou et al. 2009) or a close neighbour (Girardi et al. 1996). In the case of Abell 1691, we see that the overall profile declines gently with radius. This underscores our earlier finding of little significant sub-structure inside our cluster. However, the velocity dispersion profiles of the high- and low-mass galaxies are notably different. The high-mass galaxies demonstrate a steep decline with radius, to almost three-quarters their central value by $3r_{\text{virial}}$. On the other hand, the lower mass galaxies show a mild increase to a local maxima in $\sigma_p(R)$ at $\sim 2r_{\text{virial}}$ before slowly declining again to their central levels. Significantly, the inner r_{200} profiles for the high- and low-mass samples are $>3\sigma$ different. One immediate inference is that these two different mass populations have had significantly different accretion histories on to the cluster's potential – the higher mass ones in the centre perhaps being more recent arrivals due to their comparatively larger central $\sigma_p(R)$. This may point to sub-structure in the high-mass sample in the inner regions. Therefore, to

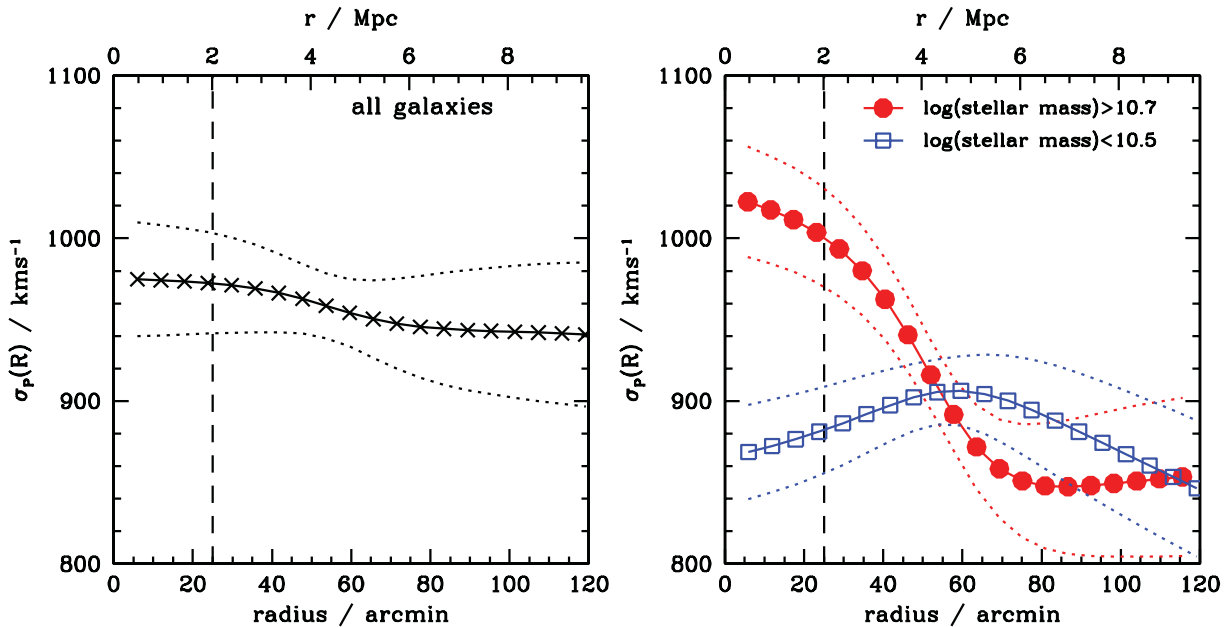


Figure 13. Velocity dispersion profile for three sets of galaxies split by mass in A1691: high-mass galaxies [$\log(\text{stellar mass}) > 10.7$; filled circles], low-mass galaxies [$\log(\text{stellar mass}) < 10.5$; open squares] and all galaxies (open circles; dotted line). For clarity, we plot these galaxies in two panels. r_{virial} is denoted by the vertical dashed line. The error bounds (dotted lines) are 1σ standard deviations derived from 1000 Monte Carlo resamplings. The high-mass sample has a significantly ($>3\sigma$) different profile to the low-mass sample within r_{virial} .

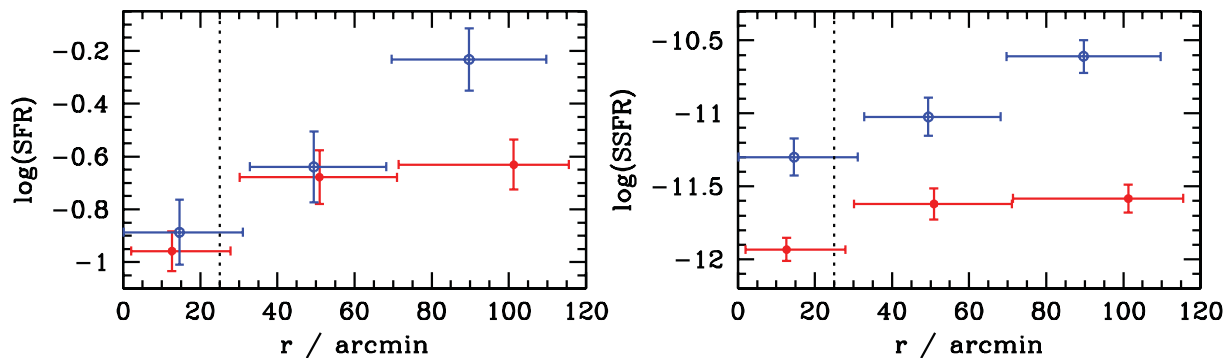


Figure 14. Star formation rate [$\log(\text{SFR})$; left] and specific star formation rate [$\log(\text{SSFR})$; right] for galaxies with high stellar mass [$\log(\text{stellar mass}) > 10.8$; filled red circles] and low stellar mass [$\log(\text{stellar mass}) < 10.5$; open blue circles] as a function of radius from the cluster centre (the vertical dotted line denotes r_{200}). Horizontal error bars denote the range of radii sampled; the vertical error bars are one standard deviation from a bootstrapped sampling of the data. The two mass regimes have significantly different forms: the higher mass galaxies quickly plateau in both plots with increasing radius.

test this, we run a DS test for the high-mass galaxies within r_{200} . We find $P(\Delta) = 0.43$, meaning that there is no significant sub-structure for the massive central galaxies. One alternative explanation is that the lower mass galaxies can have their profile flattened quicker than the higher mass galaxies following accretion on to the cluster. This would agree with the conclusions of Brough et al. (2008; see also Pimbblet 2008) who note that the time-scale for new accretion on to the cluster potential is shorter than that required to relax multiple nuclei in brightest cluster galaxies; more massive galaxies would seem more able to retain a larger peculiar (to the cluster) velocity.

7.2 Filaments, duty cycles and discussion

Filaments of galaxies have been noted in the literature as having a pre-processing role in the evolution of galaxies that are being funnelled along them to the galaxy clusters that they inter-connect (e.g. Fadda et al. 2008; Koyama et al. 2008; Porter et al. 2008). We select three of the filaments leading off the core of A1691 by a visual inspection of Fig. 3: one going north, in the direction of cluster candidate 632 of Yoon et al. (2008); the eastward extension of A1691, and the thin curved filament heading broadly south from the cluster. We investigate these three filaments, both combined and as individual objects, for trends deviating from that of the cluster as a whole but are unable to find an excess of starburst galaxies, post-starburst galaxies (k+a types), emission line types, star formation rates or specific star formation rates. On the surface, this is contrary to the results of Porter et al. (2008) and the IR study of Fadda et al. (2008). We note, however, that the Porter et al. results concern inter-cluster filaments of a straight morphology. The only filament in our sample that could fall under that category in our sample is the one running to the north of the cluster core, in the direction of cluster candidate 632 of Yoon et al. (2008). Being of the order of 5 Mpc long, this one would have been excluded from the Porter et al. sample for being too short. There is potentially an interesting inference from this null result: that filaments need a sufficient mass to pre-process galaxies and cause the enhanced star formation observed by Porter et al. A larger sample of weaker (i.e. lower mass) filaments will be able to resolve this in the future [e.g. using the Galaxy And Mass Assembly (GAMA) data set; Driver et al. 2011].

Taking the above results together, the duty cycle of lower mass galaxies appears to be distinct from higher mass ones (Haines et al. 2006; Oemler et al. 2009 and references therein; von der Linden et al.

2010). Haines et al. (2006) and von der Linden et al. (2010) both deduce a different environmental dependence for the star formation of low- versus high-mass galaxies that we are able to test using the data for A1691. In Fig. 14, we compare the star formation rates and specific star formation rates of low-mass [$\log(\text{stellar mass}) < 10.5$] and high-mass [$\log(\text{stellar mass}) > 10.7$] galaxies as a function of radius from the cluster centre for the mass-bias-corrected sample.

The two different mass regimes have significantly different forms: the high-mass galaxies plateau in both specific- and star formation rates at radii larger than r_{200} whereas the lower mass galaxies follow a strong increasing trend. These results agree well with Haines et al. (2006) who note that dwarf galaxies transition from being passive (i.e. rates consistent with massive galaxies) within R_{virial} to being highly star forming outside this radius.

Therefore, the low-mass galaxy population appear to undergo a starburst event at some distance from the cluster core (more likely a large radius), before fading into a redder population (cf. Porter et al. 2008). This starburst phase is likely to be at least partially (perhaps mainly) responsible for the Butcher–Oemler effect and therefore the effect may simply measure how efficiently low-mass galaxies are being processed by the cluster environment at this redshift.² As low-mass galaxies approach the cluster core, their star formation has likely been shut down and they will readily be undergoing morphological transformation (although the time-scale for morphological transform will be different to star formation truncation and colour change). Those lower mass systems in the centre of the cluster have a much smaller velocity dispersion profile than the high-mass ones (the inverse being true at larger radii). This suggests that the low-mass galaxies at the outskirts have recently been accreted, whereas those in the centre have had their velocity profile dampened more quickly relative to the massive galaxies that are better able to retain a higher peculiar velocity in the cluster frame.

Meanwhile for more massive galaxies, star formation appears to have been shut down a long time ago in the main part, but almost certainly shut down prior to morphological transformation and (potential) eventual merging with other red and dead cluster

²This ties into the idea of down-sizing (Cowie et al. 1996). At higher redshifts, it may be the case that more massive galaxies will be driving the Butcher–Oemler effect, but such a hypothesis requires further testing and discussion (see e.g. De Propris et al. 2003; Raichoor & Andreon 2012a,b), which is beyond the scope of this single-cluster, low-redshift study.

galaxies. Star formation in massive galaxies (when it occurs) would therefore seem to be driven by the gas reserves of the galaxies rather than through a starburst phase. We infer that the evolution of the massive galaxies is more gentle and a slow affair compared to the brutal treatment of the low-mass galaxies.

We terminate with a few caveats. There are implicit dangers in plotting various parameters as a function of distance from the cluster core due to the covariance of the changing morphological mixture of galaxies (Dressler 1980; see also Pimblet et al. 2002; Andreon 2003), projection effects (Diaferio et al. 2001; Rines et al. 2005), as well as the existence of ‘backsplash’ populations – those galaxies that are on radial orbits that have visited the high-density core regions of the cluster and subsequently been slung back to larger distances away from the centre (Gill, Knebe & Gibson 2005; Pimblet 2011). The latter two in particular may be problematic. In the case of the former, star-forming galaxies that are close to the cluster core may simply be interlopers. This means that the fractions of star-forming galaxies presented in Table 2 should be regarded as upper limits at small distances from the cluster centre. Secondly, the backsplash population can cause any gradient with distance from the cluster centre to be dampened or smeared in relation to a full three-dimensional treatment (Atlee & Martini 2012; Ellingson et al. 2001; Balogh, Navarro & Morris 2000) which would render the points further away from the cluster core in Fig. 9 as lower limits.

8 CONCLUSIONS

We have presented an investigation of the galaxy population of Abell 1691, an intermediate X-ray luminosity cluster from SDSS data. Our main conclusions can be stated as follows.

(i) We have determined new global parameters for Abell 1691, including recession velocity ($\bar{cz} = 21257 \pm 54 \text{ km s}^{-1}$) and velocity dispersion ($\sigma_{cz} = 1009_{-36}^{+40} \text{ km s}^{-1}$). The cluster is morphologically relaxed in its core regions, with no significant sub-structure within r_{200} and is ‘fed’ by multiple filaments of galaxies within which a number of sub-groups reside.

(ii) We identify AGN from a BPT diagram and show that the cluster AGN fraction increases with radius from the cluster centre and is mostly driven by massive [$\log(\text{stellar mass}) > 10.8$] galaxies.

(iii) The blue fraction of the cluster population also increases with radius away from the centre but is driven by lower mass galaxies [$\log(\text{stellar mass}) < 10.8$]. Emission line galaxies follow a similar pattern. Moreover, the emission line galaxies are found to be driven by low-mass galaxies in the cluster [especially the recently starbursting e(a) class]. This suggests that some low-mass galaxies starburst as they are accreted on to the cluster before fading to redder colours and having their morphologies transformed. Accordingly, we suggest that the Butcher–Oemler effect could therefore be a consequence of mass selection effects.

(iv) Massive galaxies are predominantly red, occupy the centre of the cluster, are non-star-forming, have a different velocity dispersion profile to other cluster galaxies and are likely to have had a significantly different duty cycle compared to the bluer galaxies. We have investigated the environment and mass of red and passive spiral galaxies (which are likely to be a transition class object) and show that they are also driven by mass but do not have a preferential position (environment) within the cluster.

This paper follows Jensen & Pimblet (2012) and is our second paper examining the ‘environment’ of intermediate L_X galaxy clusters.

ACKNOWLEDGMENTS

We would like to thank Heath Jones, Matt Owers, Stefano Andreon, Samantha Penny and Tim Dolley for helpful discussion during the course of this work. KAP thanks Iris Pimblet for inspiration. We are also particularly grateful to the anonymous referee for her/his feedback that significantly improved this work.

Fig. 5 was produced using the KARMA toolkit (Gooch 1996).

Funding for the SDSS and SDSS-II has been provided by the Alfred P. Sloan Foundation, the Participating Institutions, the National Science Foundation, the U.S. Department of Energy, the National Aeronautics and Space Administration, the Japanese Monbukagakusho, the Max-Planck Society and the Higher Education Funding Council for England. The SDSS Web site is <http://www.sdss.org/>.

The SDSS is managed by the Astrophysical Research Consortium for the Participating Institutions. The Participating Institutions are the American Museum of Natural History, Astrophysical Institute Potsdam, University of Basel, University of Cambridge, Case Western Reserve University, University of Chicago, Drexel University, Fermilab, the Institute for Advanced Study, the Japan Participation Group, Johns Hopkins University, the Joint Institute for Nuclear Astrophysics, the Kavli Institute for Particle Astrophysics and Cosmology, the Korean Scientist Group, the Chinese Academy of Sciences (LAMOST), Los Alamos National Laboratory, the Max-Planck-Institute for Astronomy (MPIA), the Max-Planck-Institute for Astrophysics (MPA), New Mexico State University, Ohio State University, University of Pittsburgh, University of Portsmouth, Princeton University, the United States Naval Observatory and the University of Washington.

This research has made use of the NED which is operated by the Jet Propulsion Laboratory, California Institute of Technology, under contract with the National Aeronautics and Space Administration.

REFERENCES

- Abazajian K. N. et al., 2009, *ApJS*, 182, 543
 Abraham R. G. et al., 1996, *ApJ*, 471, 694
 Aird J. et al., 2012, *ApJ*, 746, 90
 Alexander D. M., Hickox R. C., 2012, *New Astron. Rev.*, 56, 93
 Andreon S., 2003, *A&A*, 409, 37
 Andreon S., Davoust E., 1997, *A&A*, 319, 747
 Andreon S., Ettori S., 1999, *ApJ*, 516, 647
 Andreon S., Quintana H., Tajer M., Galaz G., Surdej J., 2006, *MNRAS*, 365, 915
 Atlee D. W., Martini P., 2012, *ApJ*, preprint (arXiv:1201.2957)
 Atlee D. W., Martini P., Assef R. J., Kelson D. D., Mulchaey J. S., 2011, *ApJ*, 729, 22
 Baldry I. K., Balogh M. L., Bower R. G., Glazebrook K., Nichol R. C., Bamford S. P., Budavari T., 2006, *MNRAS*, 373, 469
 Baldwin J. A., Phillips M. M., Terlevich R., 1981, *PASP*, 93, 5
 Balogh M. L., Morris S. L., 2000, *MNRAS*, 318, 703
 Balogh M. L., Navarro J. F., Morris S. L., 2000, *ApJ*, 540, 113
 Balogh M. L., Baldry I. K., Nichol R., Miller C., Bower R., Glazebrook K., 2004a, *ApJ*, 615, L101
 Balogh M. et al., 2004b, *MNRAS*, 348, 1355
 Bamford S. P. et al., 2009, *MNRAS*, 393, 1324
 Bekki K., Couch W. J., Shioya Y., 2001, *PASJ*, 53, 395
 Bekki K., Couch W. J., Shioya Y., 2002, *ApJ*, 577, 651
 Bergond G., Zepf S. E., Romanowsky A. J., Sharples R. M., Rhode K. L., 2006, *A&A*, 448, 155
 Blanton M. R., Lin H., Lupton R. H., Maley F. M., Young N., Zehavi I., Loveday J., 2003, *AJ*, 125, 2276
 Boselli A., Gavazzi G., 2006, *PASP*, 118, 517
 Bower R. G., Lucey J. R., Ellis R. S., 1992, *MNRAS*, 254, 601

- Branchesi M., Gioia I. M., Fanti C., Fanti R., Cappelluti N., 2007, *A&A*, 462, 449
- Brinchmann J., Charlot S., White S. D. M., Tremonti C., Kauffmann G., Heckman T., Brinkmann J., 2004, *MNRAS*, 351, 1151
- Brough S., Couch W. J., Collins C. A., Jarrett T., Burke D. J., Mann R. G., 2008, *MNRAS*, 385, L103
- Brusa M. et al., 2009, *A&A*, 507, 1277
- Bruzual G., Charlot S., 2003, *MNRAS*, 344, 1000
- Bundy K. et al., 2010, *ApJ*, 719, 1969
- Butcher H., Oemler A., Jr, 1978, *ApJ*, 226, 559
- Butcher H., Oemler A., Jr, 1984, *ApJ*, 285, 426
- Calvi R., Poggianti B. M., Fasano G., Vulcani B., 2012, *MNRAS*, 419, L14
- Carlberg R. G., Yee H. K. C., Ellingson E., 1997, *ApJ*, 478, 462
- Christlein D., Zabludoff A. I., 2005, *ApJ*, 621, 201
- Chung S. M., Eisenhardt P. R., Gonzalez A. H., Stanford S. A., Brodwin M., Stern D., Jarrett T., 2011, *ApJ*, 743, 34
- Cid Fernandes R., Stasińska G., Schlickmann M. S., Mateus A., Vale Asari N., Schoenell W., Sodré L., 2010, *MNRAS*, 403, 1036
- Clemens M. S., Bressan A., Nikolic B., Alexander P., Annibali F., Rampazzo R., 2006, *MNRAS*, 370, 702
- Constantin A., Hoyle F., Vogeley M. S., 2008, *ApJ*, 673, 715
- Cooper M. C. et al., 2006, *MNRAS*, 370, 198
- Couch W. J., Sharples R. M., 1987, *MNRAS*, 229, 423
- Couch W. J., Ellis R. S., Sharples R. M., Smail I., 1994, *ApJ*, 430, 121
- Couch W. J., Barger A. J., Smail I., Ellis R. S., Sharples R. M., 1998, *ApJ*, 497, 188
- Cowie L. L., Songaila A., Hu E. M., Cohen J. G., 1996, *AJ*, 112, 839
- Dahlén T., Fransson C., Näslund M., 2002, *MNRAS*, 330, 167
- Dahlén T., Fransson C., Östlin G., Näslund M., 2004, *MNRAS*, 350, 253
- Danese L., de Zotti G., di Tullio G., 1980, *A&A*, 82, 322
- De Propriis R., Stanford S. A., Eisenhardt P. R., Dickinson M., 2003, *ApJ*, 598, 20
- De Propriis R. et al., 2004, *MNRAS*, 351, 125
- Deng X.-F., Wen X.-Q., Xu J.-Y., Ding Y.-P., Huang T., 2010, *ApJ*, 716, 599
- di Serego Alighieri S., Lanzoni B., Jørgensen I., 2006, *ApJ*, 647, L99
- Diaferio A., Kauffmann G., Balogh M. L., White S. D. M., Schade D., Ellingson E., 2001, *MNRAS*, 323, 999
- Dressler A., 1980, *ApJ*, 236, 351
- Dressler A., Gunn J. E., 1983, *ApJ*, 270, 7
- Dressler A., Shectman S. A., 1988, *AJ*, 95, 985
- Dressler A. et al., 1997, *ApJ*, 490, 577
- Dressler A., Smail I., Poggianti B. M., Butcher H., Couch W. J., Ellis R. S., Oemler A., Jr, 1999, *ApJS*, 122, 51
- Dressler A., Oemler A., Jr, Poggianti B. M., Smail I., Trager S., Shectman S. A., Couch W. J., Ellis R. S., 2004, *ApJ*, 617, 867
- Dressler A., Rigby J., Oemler A., Jr, Fritz J., Poggianti B. M., Rieke G., Bai L., 2009, *ApJ*, 693, 140
- Driver S. P. et al., 2011, *MNRAS*, 413, 971
- Eastman J., Martini P., Sivakoff G., Kelson D. D., Mulchaey J. S., Tran K.-V., 2007, *ApJ*, 664, L9
- Ebeling H., Edge A. C., Allen S. W., Crawford C. S., Fabian A. C., Huchra J. P., 2000, *MNRAS*, 318, 333
- Ellingson E., Lin H., Yee H. K. C., Carlberg R. G., 2001, *ApJ*, 547, 609
- Fabricant D. G., Bautz M. W., McClintock J. E., 1994, *AJ*, 107, 8
- Fadda D., Biviano A., Marleau F. R., Storrie-Lombardi L. J., Durret F., 2008, *ApJ*, 672, L9
- Fisher D., Fabricant D., Franx M., van Dokkum P., 1998, *ApJ*, 498, 195
- Gallazzi A. et al., 2009, *ApJ*, 690, 1883
- Gao L., White S. D. M., Jenkins A., Stoehr F., Springel V., 2004, *MNRAS*, 355, 819
- Gavazzi G., Savorgnan G., Fumagalli M., 2011, *A&A*, 534, A31
- Georgakakis A. et al., 2008, *MNRAS*, 385, 2049
- Gill S. P. D., Knebe A., Gibson B. K., 2005, *MNRAS*, 356, 1327
- Gilmour R., Gray M. E., Almaini O., Best P., Wolf C., Meisenheimer K., Papovich C., Bell E., 2007, *MNRAS*, 380, 1467
- Giodini S. et al., 2012, *A&A*, 538, A104
- Girardi M., Fadda D., Giuricin G., Mardirossian F., Mezzetti M., Biviano A., 1996, *ApJ*, 457, 61
- Girardi M., Giuricin G., Mardirossian F., Mezzetti M., Boschin W., 1998, *ApJ*, 505, 74
- Gómez P. L. et al., 2003, *ApJ*, 584, 210
- Gooch R., 1996, in Jacoby G. H., Barnes J., eds, *ASP Conf. Ser. Vol. 101, Astronomical Data Analysis Software and Systems V. Astron. Soc. Pac., San Francisco*, p. 80
- Goto T. et al., 2003a, *PASJ*, 55, 739
- Goto T. et al., 2003b, *PASJ*, 55, 757
- Grützbauch R., Conselice C. J., Varela J., Bundy K., Cooper M. C., Skibba R., Willmer C. N. A., 2011, *MNRAS*, 411, 929
- Gunn J. E., Gott J. R., III, 1972, *ApJ*, 176, 1
- Haggard D., Green P. J., Anderson S. F., Constantin A., Aldcroft T. L., Kim D.-W., Barkhouse W. A., 2010, *ApJ*, 723, 1447
- Haines C. P., La Barbera F., Mercurio A., Merluzzi P., Busarello G., 2006, *ApJ*, 647, L21
- Haines C. P. et al., 2009, *ApJ*, 704, 126
- Heckman T. M., 1980, *A&A*, 87, 152
- Heckman T. M., Ptak A., Hornschemeier A., Kauffmann G., 2005, *ApJ*, 634, 161
- Henriksen M., Byrd G., 1996, *ApJ*, 459, 82
- Ho L. C., Filippenko A. V., Sargent W. L. W., 1997, *ApJS*, 112, 315
- Holden B. P. et al., 2007, *ApJ*, 670, 190
- Hou A., Parker L. C., Harris W. E., Wilman D. J., 2009, *ApJ*, 702, 1199
- Hou A. et al., 2012, *MNRAS*, 421, 3594
- Hwang H. S., Park C., Elbaz D., Choi Y.-Y., 2012, *A&A*, 538, A15
- Ishigaki M., Goto T., Matsuhara H., 2007, *MNRAS*, 382, 270
- Jensen P. C., Pimbblet K. A., 2012, *MNRAS*, 422, 2841
- Jester S. et al., 2005, *AJ*, 130, 873
- Johnson O., Best P. N., Almaini O., 2003, *MNRAS*, 343, 924
- Kauffmann G. et al., 2003a, *MNRAS*, 346, 1055
- Kauffmann G. et al., 2003b, *MNRAS*, 341, 33
- Kauffmann G., White S. D. M., Heckman T. M., Ménard B., Brinchmann J., Charlot S., Tremonti C., Brinkmann J., 2004, *MNRAS*, 353, 713
- Kewley L. J., Dopita M. A., Sutherland R. S., Heisler C. A., Trevena J., 2001, *ApJ*, 556, 121
- Kodama T., Bower R. G., 2001, *MNRAS*, 321, 18
- Koyama Y. et al., 2008, *MNRAS*, 391, 1758
- Lake G., Katz N., Moore B., 1998, *ApJ*, 495, 152
- Larson R. B., Tinsley B. M., Caldwell C. N., 1980, *ApJ*, 237, 692
- Lavery R. J., Henry J. P., 1988, *ApJ*, 330, 596
- Lee J. H., Lee M. G., Park C., Choi Y.-Y., 2010, *MNRAS*, 403, 1930
- Lewis I. et al., 2002, *MNRAS*, 334, 673
- Li I. H., Yee H. K. C., Ellingson E., 2009, *ApJ*, 698, 83
- Lintott C. J. et al., 2008, *MNRAS*, 389, 1179
- Lintott C. et al., 2011, *MNRAS*, 410, 166
- Lubin L. M., 1996, *AJ*, 112, 23
- Magorrian J. et al., 1998, *AJ*, 115, 2285
- Mahajan S., Raychaudhury S., 2009, *MNRAS*, 400, 687
- Mahajan S., Haines C. P., Raychaudhury S., 2010, *MNRAS*, 404, 1745
- Ma C.-J., Ebeling H., 2011, *MNRAS*, 410, 2593
- Margoniner V. E., de Carvalho R. R., 2000, *AJ*, 119, 1562
- Margoniner V. E., de Carvalho R. R., Gal R. R., Djorgovski S. G., 2001, *ApJ*, 548, L143
- Martini P., Mulchaey J. S., Kelson D. D., 2007, *ApJ*, 664, 761
- Masters K. L. et al., 2010, *MNRAS*, 405, 783
- Menci N., Fusco-Femiano R., 1996, *ApJ*, 472, 46
- Miller C. J., Nichol R. C., Gómez P. L., Hopkins A. M., Bernardi M., 2003, *ApJ*, 597, 142
- Montero-Dorta A. D. et al., 2009, *MNRAS*, 392, 125
- Moore B., Katz N., Lake G., Dressler A., Oemler A., 1996, *Nat*, 379, 613
- Moran S. M., Ellis R. S., Treu T., Salim S., Rich R. M., Smith G. P., Kneib J.-P., 2006, *ApJ*, 641, L97
- Nair P. B., Abraham R. G., 2010, *ApJ*, 714, L260
- Oemler A., Jr, Dressler A., Kelson D., Rigby J., Poggianti B. M., Fritz J., Morrison G., Smail I., 2009, *ApJ*, 693, 152
- Owers M. S., Couch W. J., Nulsen P. E. J., 2009, *ApJ*, 693, 901
- Pasquali A., van den Bosch F. C., Mo H. J., Yang X., Somerville R., 2009, *MNRAS*, 394, 38

- Pasquali A., Gallazzi A., Fontanot F., van den Bosch F. C., De Lucia G., Mo H. J., Yang X., 2010, *MNRAS*, 407, 937
- Patel S. G., Kelson D. D., Holden B. P., Franx M., Illingworth G. D., 2011, *ApJ*, 735, 53
- Peng Y.-J. et al., 2010, *ApJ*, 721, 193
- Pimbblet K. A., 2008, *PASA*, 25, 176
- Pimbblet K. A., 2011, *MNRAS*, 411, 2637
- Pimbblet K. A., Smail I., Kodama T., Couch W. J., Edge A. C., Zabludoff A. I., O'Hely E., 2002, *MNRAS*, 331, 333
- Pimbblet K. A., Drinkwater M. J., Hawkrigg M. C., 2004, *MNRAS*, 354, L61
- Pimbblet K. A., Smail I., Edge A. C., O'Hely E., Couch W. J., Zabludoff A. I., 2006, *MNRAS*, 366, 645
- Pinkney J., Roettiger K., Burns J. O., Bird C. M., 1996, *ApJS*, 104, 1
- Poggianti B. M., Smail I., Dressler A., Couch W. J., Barger A. J., Butcher H., Ellis R. S., Oemler A., Jr, 1999, *ApJ*, 518, 576
- Poggianti B. M., Bressan A., Franceschini A., 2001, *ApJ*, 550, 195
- Popesso P., Biviano A., 2006, *A&A*, 460, L23
- Popesso P., Biviano A., Böhringer H., Romaniello M., Voges W., 2005, *A&A*, 433, 431
- Porter S. C., Raychaudhury S., Pimbblet K. A., Drinkwater M. J., 2008, *MNRAS*, 388, 1152
- Press W. H., Teukolsky S. A., Vetterling W. T., Flannery B. P., 1992, *Numerical Recipes*. Cambridge Univ. Press, Cambridge
- Quilis V., Moore B., Bower R., 2000, *Sci*, 288, 1617
- Raichoor A., Andreon S., 2012a, *A&A*, 537, A88
- Raichoor A., Andreon S., 2012b, *A&A*, 543, A19
- Rakos K. D., Schombert J. M., 1995, *ApJ*, 439, 47
- Rines K., Geller M. J., Kurtz M. J., Diaferio A., 2005, *AJ*, 130, 1482
- Rood H. J., Page T. L., Kintner E. C., King I. R., 1972, *ApJ*, 175, 627
- Ruderman J. T., Ebeling H., 2005, *ApJ*, 623, L81
- Sato T., Martin C. L., 2006, *ApJ*, 647, 946
- Sivakoff G. R., Martini P., Zabludoff A. I., Kelson D. D., Mulchaey J. S., 2008, *ApJ*, 682, 803
- Skibba R. A. et al., 2009, *MNRAS*, 399, 966
- Smail I., Edge A. C., Ellis R. S., Blandford R. D., 1998, *MNRAS*, 293, 124
- Spergel D. N. et al., 2007, *ApJS*, 170, 377
- Stasińska G., Cid Fernandes R., Mateus A., Sodré L., Asari N. V., 2006, *MNRAS*, 371, 972
- Strauss M. A. et al., 2002, *AJ*, 124, 1810
- Tajiri Y. Y., Kamaya H., 2001, *ApJ*, 562, L125
- Thomas D., Maraston C., Schawinski K., Sarzi M., Silk J., 2010, *MNRAS*, 404, 1775
- Tran K.-V. H., Franx M., Illingworth G., Kelson D. D., van Dokkum P., 2003, *ApJ*, 599, 865
- Tran K.-V. H., van Dokkum P., Illingworth G. D., Kelson D., Gonzalez A., Franx M., 2005, *ApJ*, 619, 134
- Tremonti C. A. et al., 2004, *ApJ*, 613, 898
- Urquhart S. A., Willis J. P., Hoekstra H., Pierre M., 2010, *MNRAS*, 406, 368
- van den Bosch F. C., Pasquali A., Yang X., Mo H. J., Weinmann S., McIntosh D. H., Aquino D., 2008, *MNRAS*, preprint (arXiv:0805.0002)
- van der Wel A. et al., 2007, *ApJ*, 670, 206
- van Dokkum P. G., Franx M., Fabricant D., Kelson D. D., Illingworth G. D., 1999, *ApJ*, 520, L95
- Veilleux S., Osterbrock D. E., 1987, *ApJS*, 63, 295
- Visvanathan N., Sandage A., 1977, *ApJ*, 216, 214
- von der Linden A., Wild V., Kauffmann G., White S. D. M., Weinmann S., 2010, *MNRAS*, 404, 1231
- Vulcani B. et al., 2012, *A&A*, preprint (arXiv:1111.0830)
- Wetzel A. R., Tinker J. L., Conroy C., 2012, *MNRAS*, 424, 232
- Wilman D. J., Erwin P., 2012, *ApJ*, 746, 160
- Wilman D. J., Zibetti S., Budavári T., 2010, *MNRAS*, 406, 1701
- Wolf C. et al., 2009, *MNRAS*, 393, 1302
- Xue Y. Q. et al., 2010, *ApJ*, 720, 368
- Yahil A., Vidal N. V., 1977, *ApJ*, 214, 347
- Yoon J. H., Schawinski K., Sheen Y.-K., Ree C. H., Yi S. K., 2008, *ApJS*, 176, 414
- Zabludoff A. I., Huchra J. P., Geller M. J., 1990, *ApJS*, 74, 1
- Zabludoff A. I., Zaritsky D., Lin H., Tucker D., Hashimoto Y., Shectman S. A., Oemler A., Kirshner R. P., 1996, *ApJ*, 466, 104

This paper has been typeset from a $\text{\TeX}/\text{\LaTeX}$ file prepared by the author.